Density functional theory guided advances in phase-change materials and memories

Wei Zhang[1,2]*, Volker L. Deringer[3], Richard Dronskowski[3,5], Riccardo Mazzarello[4,5], Evan Ma[1,6] and Matthias Wuttig[2,5]

[1]Center for Advancing Materials Performance from the Nanoscale, State Key Laboratory for Mechanical Behavior of Materials, Xi'an Jiaotong University, Xi'an 710049, PR China
[2]I. Institute of Physics (IA), RWTH Aachen University, 52056 Aachen, Germany
[3]Institute of Inorganic Chemistry, RWTH Aachen University, Landoltweg 1, 52056 Aachen, Germany
[4]Institute for Theoretical Solid-State Physics, RWTH Aachen University, 52074 Aachen, Germany
[5]Jülich-Aachen Research Alliance (JARA-FIT and JARA-HPC), RWTH Aachen University, 52056 Aachen, Germany
[6]Department of Materials Science and Engineering Johns Hopkins University Baltimore, MD 21218, USA

*Contact Author, wzhang0@mail.xjtu.edu.cn

Abstract

Phase-change materials (PCMs) are promising candidates for novel data-storage and memory applications. They encode digital information by exploiting the optical and electronic contrast between amorphous and crystalline states. Rapid and reversible switching between the two states can be induced by voltage or laser pulses. Here, we review how density functional theory (DFT) has been, and is, advancing our understanding of PCMs. We describe key DFT insights into structural, electronic and bonding properties of PCMs, and into technologically relevant processes such as fast crystallization and relaxation of the amorphous state. We then comment on the leading role played by predictive DFT simulations for new potential applications of PCMs, including topological insulating properties, switching between different topological states, and magnetic properties of doped PCMs. Such DFT-based approaches are also projected to be powerful in guiding advances in other materials-science fields.

Keywords: amorphous, electronic material, memory, phase transformation, simulation

Introduction

The global demand for data storage is growing ever faster in the "information age". Silicon-based Flash memories, which dominated the non-volatile storage market so far, seem to have reached their performance and scalability limits, and massive efforts are underway to develop new memory materials. Amidst them, phase-change random access memory (PRAM) based on PCMs shows great promise[1,2,3,4]: a universal device[5] could be realized if superior materials can be identified, which could potentially replace magnetic hard drives, Flash memories and DRAM.

The storage concept of PCMs is sketched in **Figure 1**. At room temperature, these materials possess at least two metastable phases, amorphous and crystalline, with pronounced contrast in optical reflectivity and electrical resistance; this represents the two logic states, "0" and "1". By applying a long, medium-intensity voltage or laser pulse, the amorphous region is locally annealed and crystallized ("SET"). Using a short, high-intensity voltage or laser pulse, the focused region is instead heated above its melting temperature; subsequent rapid cooling yields a disordered amorphous mark ("RESET"). To read out information, a small current pulse or laser beam is used that does not alter the state of the bit[1,3].

The most successful candidates for phase-change technology locate in the ternary Ge–Sb–Te system[1,3] (**Figure 1e**). There are three main families: tellurides along the quasi-binary GeTe–Sb_2Te_3 tie-line ("GST" in the sequel), alloyed or, in the community's jargon, "doped" Sb_2Te (prominently, Ag–In–Sb–Te alloys), and derivatives of elemental antimony such as $Ge_{15}Sb_{85}$. Some emerging electronic data-storage and memory products that employ PCMs are shown in **Figure 1f**.

Computer simulations play key roles in modern materials science. They have been supplementing experiments for long, and are now unfolding truly predictive power. DFT-based electronic-structure theory[6] and molecular-dynamics[7] (DFMD) simulations can characterize "real" materials with quantum-mechanical accuracy, without

the need of any experimental input. Thanks to the exponential growth of supercomputing power, state-of-the-art simulations can now access the time- and length-scales of the physical processes in phase-change memory cells.

In this overview article, we summarize DFT-guided advances in the materials science of PCMs and in PRAM technology. We have compiled a list of questions, which, in our opinion, address several crucial issues regarding PCMs. Some of the questions have been resolved, and some are still being pursued. Answering them will also inspire important advances beyond the field of PCMs.

What makes crystalline and amorphous PCMs so different?

The first and quick answer is "structure". While atomic structure is very important, there is even more than that. The different properties of the two phases are caused by very complex aspects on the atomic scale that have recently been reviewed[8]. Albeit current research is focusing on electronic memories, the most important consumer products based on PCMs so far have been *optical* disks (e.g., re-writeable Blu-ray); naturally, many studies have been devoted to the optical property contrast of PCMs. Based on experiments[9] and later corroborated by theory10,11, it was suggested that crystalline PCMs are characterized by a generic bonding mechanism—resonance bonding, which originates from the resonance between different bonding configurations. This mechanism leads to electron delocalization and high dielectric constants. The misalignment of directional *p* bonds weakens resonance bonding and, thus, lowers the dielectric constant and changes the optical matrix elements significantly11. As angular disorder in *p*-bonding prevails in amorphous PCMs[12], the origin of the optical contrast is thus identified. It is such microscopic understanding that paves the way to discover new PCMs with optimal properties[10].

Metastable GST alloys form rocksalt-type structures upon fast crystallization, with a fully occupied Te sublattice and an interpenetrating one on which Ge, Sb, and

vacancies are randomly arranged[13,14]. Why is this stoichiometric amount of vacancies formed, in the first place? This question was addressed using DFT[15]—first, computing energies, then, dissecting the electronic structures with the help of a quantum-chemical bonding indicator, dubbed crystal orbital Hamilton population (COHP)[16] analysis. Starting from a hypothetical rocksalt $Ge_2Sb_2Te_4$ alloy, Ge atoms were gradually taken out of the model structure, until arriving at the experimentally observed composition $Ge_1Sb_2Te_4$ (**Figure 2a,c**). Large negative formation energies were found, already suggesting that the presence of vacancies is favorable, but the full *understanding* came from bonding theory (**Figure 2b,d**). The hypothetical, fully occupied lattice of $Ge_2Sb_2Te_4$ exhibits significant antibonding interactions ($-COHP < 0$) at the Fermi level E_F, which decrease when Ge atoms are removed; this is because the cationic atoms donate electrons to the host structure. Nonetheless, a certain amount of occupied, antibonding levels remains in $Ge_1Sb_2Te_4$, and similar observations have been made for the binary parent compounds GeTe[17] and Sb_2Te_3[18].

What causes the electronic contrast?

Both amorphous and cubic GST are semiconducting with band gaps of 0.5–1.0 eV. Nevertheless, at room temperature, the electrical resistance values of the two metastable phases differ by more than three orders of magnitude[19]. This contrast stems from the interplay between disorder strength and carrier concentration. In the amorphous state, E_F is pinned in the middle of the band gap due to disorder, and the carrier concentration is low. Rocksalt GST and related materials, on the other hand, exhibit so-called *self-doping* and p-type conductivity. This behavior has been traced back to the presence of excess Ge/Sb vacancies (that is, beyond those shown in Figure 2c) in DFT-based studies[20,21]. Consequently, E_F is shifted to the valence band and large concentrations of hole carriers arise[19].

Interestingly, upon further thermal annealing of crystalline GST, the electrical resistance decreases by another three orders of magnitude at room temperature[19].

Low-temperature transport measurements also revealed exciting phenomena: namely, disorder-induced electron localization and metal–insulator transitions[19,22]. In Reference 23, Zhang *et al.* elucidated their microscopic origin by large-scale DFT simulations. Rocksalt-type and pseudo-hexagonal structural models of GST, containing up to 3,584 atoms, were subjected to DFT. Anderson localization was observed in the disordered models (**Figure 2f**): computing atomic projections of the electronic density of states, the inverse participation ratio (IPR), and the spatial distribution of electronic wavefunctions, it was shown that the states near E_F are exponentially localized inside vacancy-rich regions. The simulations also indicated that vacancy clusters order into vacancy planes upon progressive thermal annealing, which drives the structural transition from cubic to layered structures, and, independently, leads to extended electronic states and metallic behavior (**Figures 2e,g**).

How does one simulate an amorphous material?

If crystalline PCMs are complex already, this holds even more so for their amorphous (glassy) counterparts. The first DFMD simulations of amorphous PCMs were reported independently by Caravati *et al.*[24] and Akola *et al.*[25] in 2007. Amorphous (a-) $Ge_2Sb_2Te_5$ and GeTe were produced by a melt-quench scheme: a simulation cell is loaded with atoms, randomized at very high temperature, then rapidly cooled down to achieve an amorphous structure (**Figure 3a**). The X-ray scattering factor $S(q)$ was calculated based on the trajectory of a-GST at room temperature and compared to experiments[24] (**Figure 3b**): clearly, the overall shape and primary peak positions of $S(q)$ are well recovered. DFMD simulations also allow one to determine quantities that are *not* easily accessible experimentally. The analysis of primitive rings, a typical indicator for medium-range order, revealed that four-fold rings dominate over the others, and most rings are planar with ABAB patterns (A-Ge/Sb, B-Te)[24,25,26] (**Figure 3c**). Besides, vacancy voids are abundant in amorphous PCMs[25,27,28] (**Figure 3d**). Both observations were suggested to be linked to the materials' fast crystallization capability.

Local structural motifs in amorphous PCMs have been under very active study since a seminal paper by Kolobov *et al.*[29] in 2004. From extended X-ray absorption fine-structure spectroscopy (EXAFS) and X-ray absorption near-edge structure (XANES) spectra of amorphous and recrystallized GST, the authors proposed an umbrella-flip model in which Ge atoms switch back and forth between octahedral and interstitial tetrahedral sites. This model provided an intuitive picture of the phase transitions; nevertheless the real processes turn out to be far more complex. In DFMD simulations of melt-quenched *a*-GST[24,25] only roughly one third of Ge atoms is found in tetrahedral environments (denoted Ge^T), whereas the residual Ge atoms take defective octahedral configurations (Ge^O; **Figure 4a**), as do all Sb and Te atoms. Coordination numbers and nearest-neighbor bond lengths can be extracted independently from EXAFS measurements and DFMD simulations: the results agree fairly well, except that the simulated Ge–Te bond length is about 6% larger than the experimental one. Unfortunately, an ultimate verdict based either on EXAFS (which involves indirect observations) or on DFT (which may have intrinsic shortcomings) is highly difficult, especially when it comes to small structural variations. In particular, the aforementioned bond-length deviation as well as the existence of Ge^T and the nature of bonding have been under debate for more than a decade.[30,31,32,33,34,35,36,37,38,39]

Indeed, the observation of Ge^T in a-GeTe and a-GST is puzzling, as such motif cannot be found in any crystalline (that is, *stable*) form of the compounds: octahedral-like coordination prevails exclusively. Furthermore, most Ge^T atoms in the amorphous phase are predicted to form at least one homopolar Ge–Ge bond[24], again at variance with the crystalline phases. In 2014, a new chemical approach was used to study the local nature of these different structural fragments[40]. The tool is conceptually similar to previous COHP analyses (Figure 2), but different in detail: here, the local chemical information was extracted from numerically efficient plane-wave basis sets[41,42], which are routinely used in DFMD simulations of PCMs and other amorphous materials. In this work, the importance of homopolar bonds in stabilizing Ge^T fragments could be addressed and quantified. Figure 4b compares

projected crystal orbital overlap populations (pCOOPs) for various Ge^T and Ge^O units in a-GeTe. Obviously, Ge^T exhibit antibonding interactions at E_F, but these drop significantly with the onset of homopolar Ge–Ge bonding, while there is no pronounced change in the bonding nature of Ge^O. Since the heat of formation of GeTe is small, homopolar bonds *are* present in the molten state, and upon subnanosecond quenching, these bonds are frozen in and give rise to a fraction of Ge^T units[43]. Hence, Ge^T is ultimately transient in nature, as discussed further below.

Resistance drift (the increase of R over time) in amorphous PCMs[44,45] is an outstanding problem for both fundamental research and memory technology, as it hinders multi-level storage applications. Since this drift occurs on timescales of seconds, minutes, or days, it is inaccessible to "brute-force" DFMD simulations. Nonetheless, other approaches are possible, and recently allowed Raty *et al.*43 to identify the microscopic origin of drift in a-GeTe, based on DFT simulations. Employing the chemical substitution method[33,37], the authors generated structural models of a-GeTe, in which the fraction of Ge^T ranged from 10% to 90% (**Figure 4c**). The models with the lowest amount of Ge^T yield the lowest energy (violet points); importantly, they are more stable than "standard" melt-quenched a-GeTe models (green points). Thus, a-GeTe should evolve towards a network with less Ge^T. This lowers the energy and stress of the system, and it removes localized mid-gap electronic states. It was also shown in Reference 43 that, concomitantly, the Peierls distortion of the amorphous network increases. As a result, the optical band gap rises, and thus does the resistance, whereas the dielectric constant is lowered[46,47].

What can DFT tell us about switching kinetics — and what not?

The crystallization speed of PCMs spans over 17 orders of magnitude: at room temperature, the amorphous phases are metastable for decades, while at elevated temperatures (600-700 K) they crystallize within nanoseconds. This property is essential for data storage. Current supercomputers have made DFMD simulations of ~1,000-atom models feasible, with runs over nanoseconds[48,49]; in other words, the

crystallization process at high temperature can be directly simulated. Two different crystallization mechanisms have been identified in PCMs[50], namely nucleation and growth, as sketched in **Figure 5**. In 2008, Hegedüs and Elliott[26] achieved the first DFMD crystallization simulation of a nucleation-dominated PCM, $Ge_2Sb_2Te_5$, using a system size of 63-90 atoms. Later, the same group[51] crystallized a larger 180-atom model, which enables a reasonable estimate of critical nucleus size (24-44 atoms) and growth rate (~5 m/s). The fast crystallization was attributed to the high density of planar four-fold ABAB rings. This point was partly challenged by Kalikka *et al.*[48,52], who reported that the ABAB squares can break and reform during crystallization due to the diffusive nature of Ge/Sb/Te motion at high temperatures, and that the high atomic mobility is a prerequisite for fast growth. Their simulations comprise 460-648 atoms, and representative snapshots of the crystallization trajectory are shown in **Figure 5a**.

In 2015, Ronneberger *et al.*[53] employed metadynamics[54], an enhanced sampling technique, to accelerate the formation of critical nuclei. Within a 460-atoms supercell, quasi-spherical crystal clusters of ≤100 atoms were found stable. Crystal growth at the interface was studied as well: the estimated growth speed (~ 1 m/s) agrees reasonably with recent experiments[55,56,57]. All these simulations have shown that the pronounced disorder in metastable rocksalt GST is a consequence of the fast crystallization. The atoms near the crystal surface have very limited time to arrange themselves to impinge on the crystalline interface, and so a highly disordered structure results. Based on DFT total energy calculations, Sun *et al.*[58] and Da Silva *et al.*[59] proposed an ordered rocksalt GST with regular atomic and vacancy layers. Given enough time to guarantee a smooth crystal growth process, such phase may also be produced, e.g. by using molecular beam epitaxy technique[60].

Recently, it was shown that the crystallization time limit of GST can be further reduced by applying a constant low voltage during the crystallization process[61]. DFMD simulations indicate that this reduction stems from structural pre-ordering induced by voltage[61]. To further increase the accessible system size, Sosso *et al.*[62]

developed a DFT-trained neural-network potential obtained by fitting the GeTe hypersurface, which afforded new atomistic insight into the atomic-scale processes during crystallization of this compound[63,64].

As mentioned in the Introduction, an Ag-/In-substituted Sb_2Te alloy (AIST) is a powerful material for data storage. Different from the nucleation process in GST, the dominant crystallization mechanism of AIST is growth from the amorphous-crystalline interface (**Figure 5b**). In 2014, Zhang *et al.*[49] performed DFMD simulations of AIST crystallization, using up to 810-atom systems. As AIST crystallizes in the A7 structure[65], two adjacent crystalline layers along [0001] were fixed during the melt-quench run, creating two amorphous–crystalline boundaries. Upon heating at 585 K, the system quickly crystallized and smooth growth along the boundary was observed (**Figure 5b**); the thus obtained growth rate and recrystallized structure agreed with recent experiments[66,65]. The fast growth was explained by the high atomic mobility near the very thin interface, together with a very effective sticking process[49].

Despite these successes, DFMD simulations encountered a serious problem at lower temperatures of 450–500K: there, the obtained growth speed values are orders of magnitude larger than experimental ones[49]. This problem is attributed to the ultrahigh fragility of AIST[66] and the too fast quenching rates employed in DFMD simulations, which are typically 100-1000× higher than experimental ones (due to the very high computational cost). The potential energy landscape of fragile systems is very complex[67], and the fast quenching rates lead to insufficient exploration of phase space[49]. Therefore, at low temperatures, the simulated crystal growth is much faster than in reality.[66] As such, the crystallization dynamics at lower temperatures still remains an open question. Note that the understanding of fragility is crucial for phase-change data storage: high fragility guarantees a drastic change in the temperature dependence of the growth velocity, which makes the crystallization process ultrafast at high T, but extremely slow at room temperature[49,56,57,66].

Which challenges and opportunities lie ahead?

Finally, we mention a few new applications of PCMs in which DFT simulations also play a leading role. The structural parent compound Sb_2Te_3 is among the best-known topological insulators (TIs), [68,69] which represent a new class of electronic materials with an insulating bulk state and a topologically protected surface state (due to time-reversal symmetry and strong spin–orbit coupling)[69]. Interestingly, layered $Ge_2Sb_2Te_5$ in Petrov sequence has been predicted to be a TI:[70] the DFT band structure of the bulk phase has a finite band gap, while the surface states display metallic behavior and form a Dirac cone at the Γ point (**Figure 6a**).

Recently, Simpson, Tominaga, and coworkers[71,72] designed a new storage scheme that exploits fast and reversible transitions occurring in crystalline $Ge_2Sb_2Te_5$ superlattices. This concept, dubbed interfacial phase change memory (iPCM), could lead to significantly lower power consumption[71]. Although the switching mechanism is not fully understood, it is believed that it is due to transitions between different stacking sequences (**Figure 6b**). The contrast in electrical resistance could originate from the different topological properties of the relevant phases[70,72,73]. For this reason, iPCMs are also referred to as topological-switching random access memories (TRAM). Therefore, a DFT-based understanding of the topological properties of GST compounds is not only theoretically interesting, but also of practical value.

The properties of PCMs can be enhanced and expanded by doping with small amounts of adatoms: exploring and designing suitable dopants offers intriguing possibilities for experimental–theoretical collaboration. For example, Prasai *et al.*[74] Skelton *et al.*[75] and Zhu *et al.*[76] showed that Ag, Bi and Ti addition, respectively, can improve the crystallization kinetics of GST and Sb_2Te_3 at high temperatures. It was reported by Song *et al.*[77] that Fe doped GST is ferromagnetic in both phases, which, however, display pronounced contrast in saturation magnetization (~30%). Hence, doping with transition-metal atoms may lead to magnetic switching in

PCMs (mPCM). Design rules on dopant selection for mPCMs have been recently proposed based on DFT simulations[78,79,80].

What might other materials-science fields learn from these examples?

Before closing, we note that the experience gained and lessons learnt from employing DFT calculations in the thriving field of phase-change materials and memories, through both successful and failed attempts, could be instructive to the materials-science community at large. The specific examples discussed above are illustrative of the power of DFT-based approaches: systematic simulations to construct design rules to find better-performance compounds; large-scale DFT simulations to uncover new physics, such as disorder-induced phenomena and crystallization kinetics of complex systems (ternary, quaternary etc.); enhanced sampling techniques for rare events like nucleation; DFT-trained neural-network potentials to reduce computational costs; quenching time issues on the kinetic properties of fragile systems; electronic-level understanding of the chemical bonding nature of highly disordered amorphous materials; the use of chemical substitution methods to describe relaxation mechanisms in the amorphous state; detecting unusual electronic properties of topological phases and the switching processes between them; tailoring materials performance via doping and manipulating magnetic properties with phase-change cycles.

We believe that many other materials-science fields would benefit from similar tactics. For instance, extending our analysis of the crystallization of PCM glass discussed earlier, large-scale DFMD simulations might unravel the atomistics of crystallization kinetics (propagation speed of crystal front) in elemental metallic glasses[81], which have so far remained unexplainable using all current models and MD simulations. State-of-the-art DFT calculations are also instrumental in uncovering the unprecedented impact of defects on the electronic structure of two-dimensional materials[82,83]. *Ab initio* design rules can be developed in many fields, including engineering materials like steels[84]. Local bonding analysis method should shed

light on the understanding of other complex amorphous materials[85]. Incidentally, in this endeavor PRAM-equipped supercomputers may very well turn out to be the enabling vehicle that makes these developments feasible in the near future.

Acknowledgments

W.Z., V.L.D., R.D., R.M., and M.W. gratefully acknowledge funding from Deutsche Forschungsgemeinschaft (DFG) within SFB 917 ("Nanoswitches") as well as ERC Advanced Grant *Disorder Control* (M.W.). W.Z. gratefully thanks the Young Talent Support Plan of Xi'an Jiaotong University. E.M. acknowledges support from US DoE-BES-DMSE, DE-FG02-09ER46056.

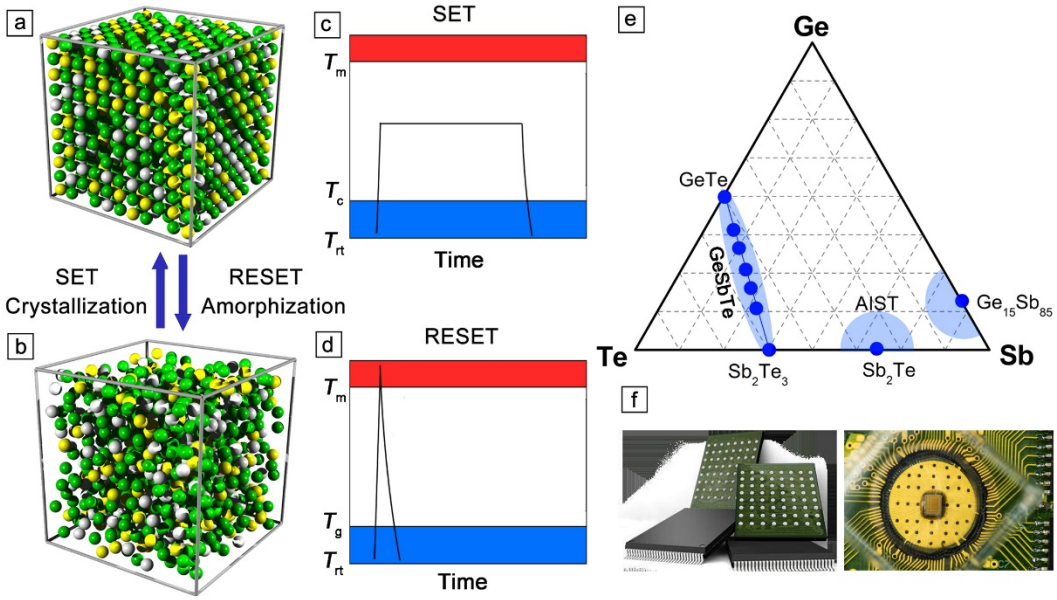

Figure 1 Working principle of PCM-based devices. The heating process is induced either by a laser or by a voltage pulse. (e) The Ge-Sb-Te ternary diagram, in which many phase change materials are located (blue). (f) Some emerging electronic data-storage and memory products that employ PCMs. © Micron Technology, Inc. and IBM.

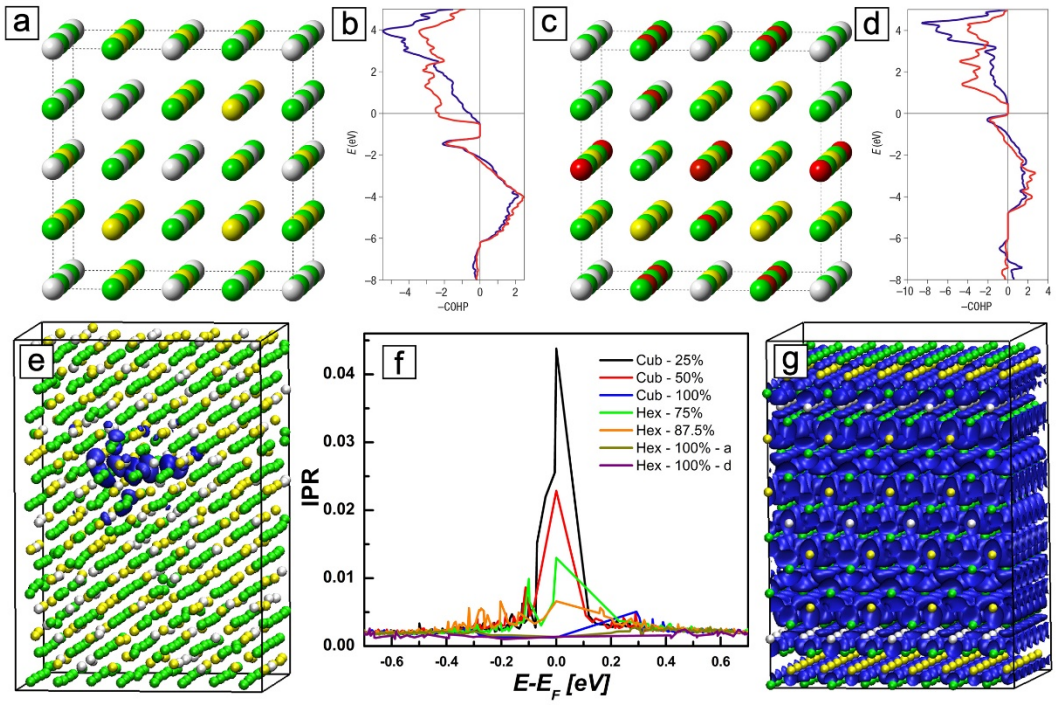

Figure 2 Adapted from Reference 15, 23. Structural and electronic properties of crystalline GeSbTe compounds, illustrating why the stoichiometric vacancies form (panels a–d) and how they influence the electronic nature by causing disorder-induced localization (panels e–g). Te, Ge, Sb and vacancies are rendered with green, grey, yellow and red spheres. (a) and (c) depict idealized crystal structures of rocksalt-type $Ge_2Sb_2Te_4$ and $Ge_1Sb_2Te_4$. The corresponding COHP curves are shown in (b) and (d) and the blue (red) curve represents Ge-Te (Sb-Te) interactions, respectively. (f) IPR curves of various disordered and ordered crystalline GST models, which serve as a measure for the regular or irregular distribution of electronic density (high IPR values indicate localization). (e) and (g) are real-space isosurfaces (blue surfaces), enclosing the highest occupied electronic levels (that is, at the Fermi level E_F) in disordered and ordered $Ge_1Sb_2Te_4$.

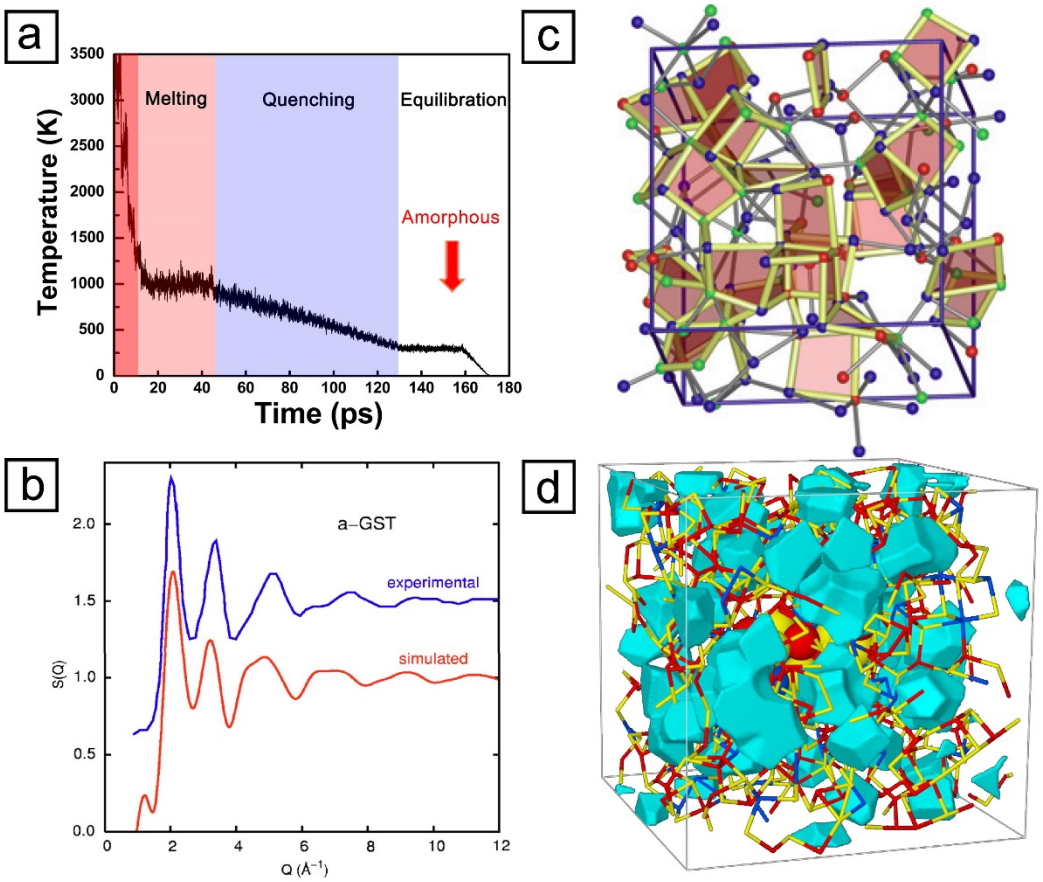

Figure 3 (a) The melt-quench scheme, illustrated by the course of simulation temperature during a "real-life" DFMD simulation. (b) Adapted from Reference 24. Comparisons of experimental and simulated X-ray structure factors $S(q)$ for amorphous $Ge_2Sb_2Te_5$. (c) Adapted from Reference 26. Planar four-fold ABAB rings in amorphous $Ge_2Sb_2Te_5$. (d) Adapted from Reference 27. Amorphous $Ge_8Sb_2Te_{11}$ with teal isosurfaces enclosing atomic vacancy voids. © 2007 American Institute of Physics, 2008 Nature Publishing Group, 2009 American Physical Society.

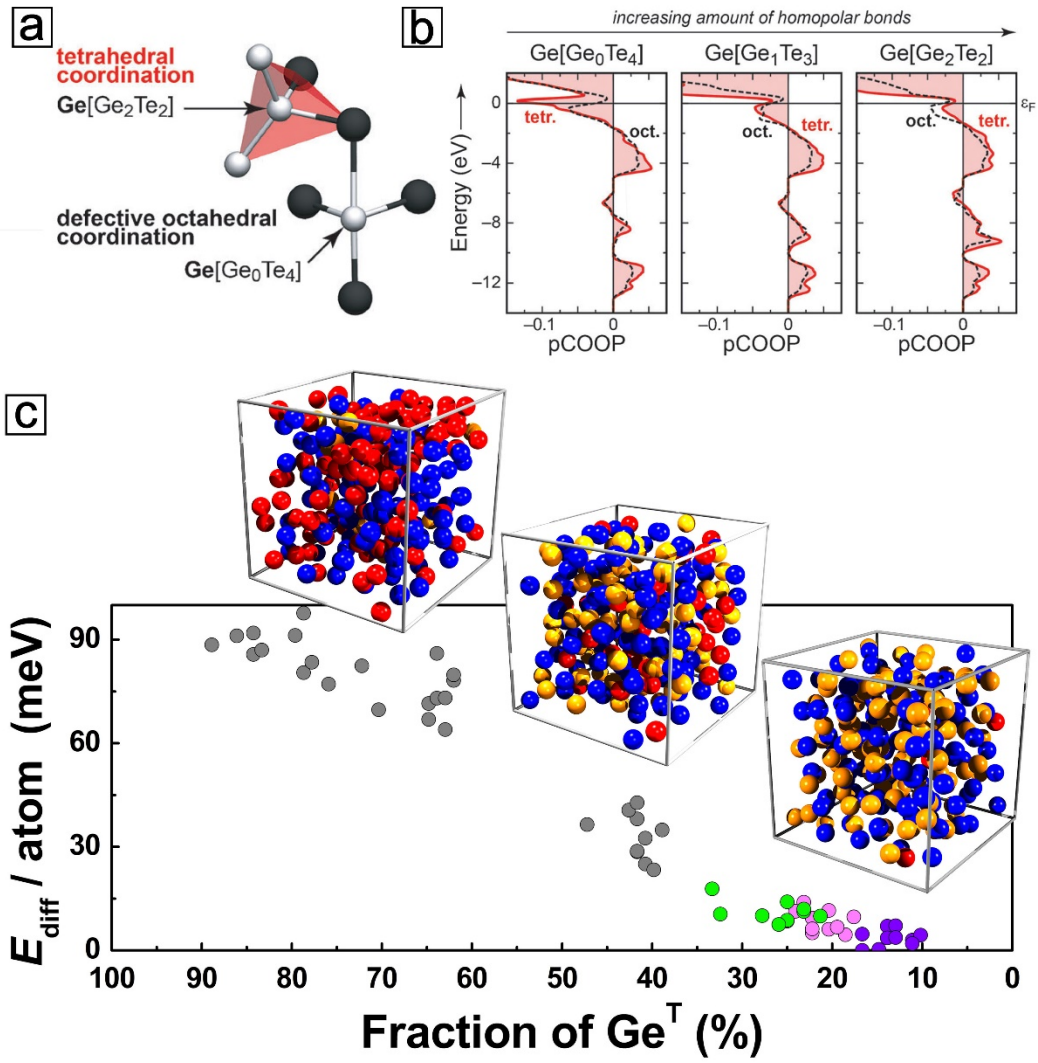

Figure 4 (a) Adapted from Reference 40. Ge^{T} and Ge^{O} motifs in a-GeTe. (b) pCOOP analysis of local stability for Ge^{T} and Ge^{O} units having different amount of homopolar Ge-Ge bonds. (c) Adapted from Reference 43. The energy hierarchy of a-GeTe with respect to the fraction of Ge^{T}. Green points present melt-quench a-GeTe, while other points were obtained by substituting Ge or Te atoms from a-SnTe (violet), a-GeSe (light magenta) and a-SiTe (grey). Three typical atomic images of a-GeTe. Ge^{T}, Ge^{O} and Te atoms are rendered with red, orange and blue spheres, respectively.

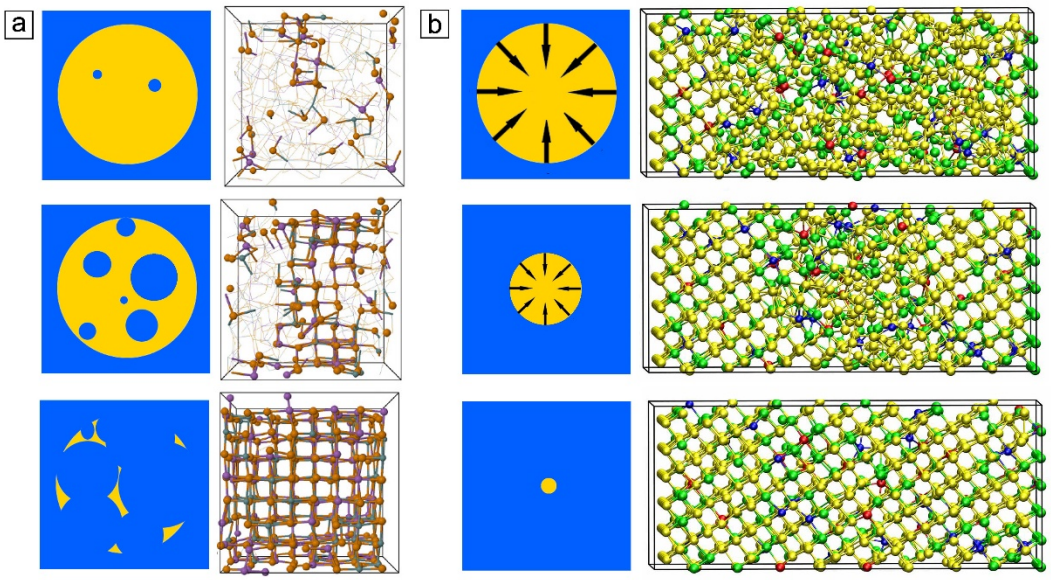

Figure 5 Crystallization kinetics of PCMs. The sketch plots are inspired by Reference 50. (a) Adapted from Reference 48. The DFMD crystallization simulations of $Ge_2Sb_2Te_5$ at 600K. Ge, Sb and Te atoms are rendered with green, purple, and orange spheres, respectively. (b) Adapted from Reference 49. The DFMD crystallization simulations of AgInSbTe at 585K. Ag, In, Sb and Te atoms are rendered with blue, red, yellow and green spheres, respectively.

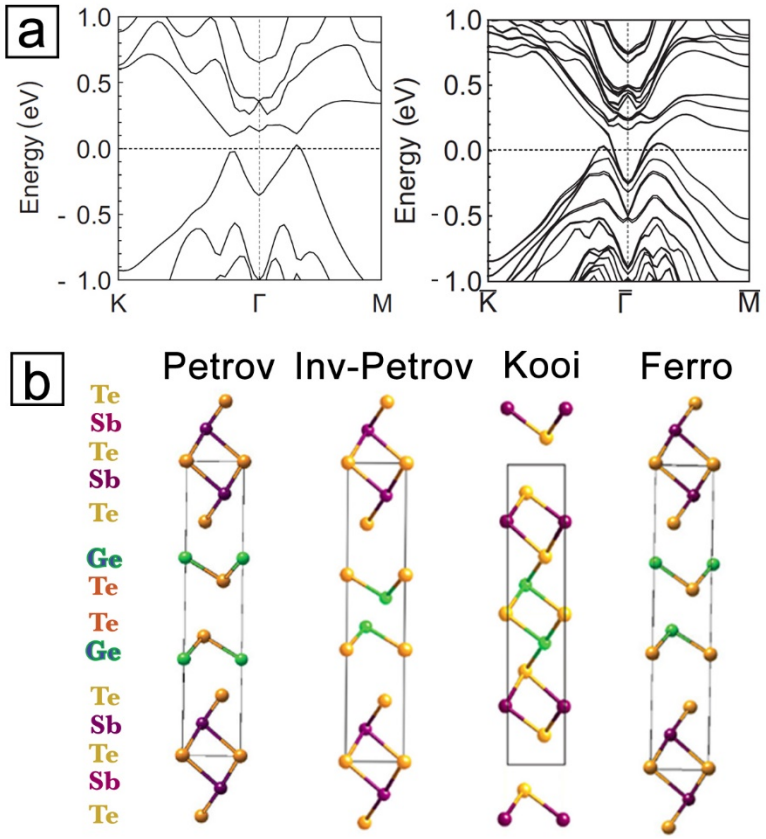

Figure 6 (a) Adapted from Reference 70. The DFT simulated electronic band structures of the bulk and surface states of hexagonal $Ge_2Sb_2Te_5$ in "Petrov" sequence. (b) Adapted from Reference 72. Possible (transient) stacking sequence of iPCM $Ge_2Sb_2Te_5$, namely, "Petrov", "inverted Petrov, "Kooi and "Ferro-GeTe". © 2010 American Physical Society, 2014 Wiley-VCH Verlag GmbH & Co. KGaA, Weinheim.

References

1. M. Wuttig, N. Yamada, *Nat. Mater.* **6**, 824 (2007)
2. T. Siegrist, P. Merkelbach, M. Wuttig, *Annu. Rev. Cond. Matt. Phys.* **3**, 215 (2012)
3. S. Raoux, F. Xiong, M. Wuttig, E. Pop, *MRS Bulletin* **39**, 703 (2014)
4. S. R. Elliott, *Int. J. Appl. Glass Sci.* **6**, 15 (2015)
5. M. H. Lankhorst, B. W. Ketelaars, R. A. Wolters, *Nat. Mater.* **4**, 347 (2005)
6. R. M. Martin *Electronic Structure: Basic Theory and Practical Methods*,
7. D. Marx, J. Hutter, *Ab Initio Molecular Dynamics: Basic Theory and Advanced Methods*,
8. V. L. Deringer, R. Dronskowski, M. Wuttig, *Adv. Funct. Mater.* , DOI: 10.1002/adfm.201500826 (2015)

9. K. Shportko, S. Kremers, M. Woda, D. Lencer, J. Robertson, M. Wuttig, *Nat. Mater.* **7**, 653 (2008)
10. D. Lencer, M. Salinga, B. Grabowski, T. Hickel, J. Neugebauer, M. Wuttig, *Nat. Mater.* **7**, 972 (2008)
11. B. Huang, J. Robertson, *Phys. Rev. B* **81**, 081204(R) (2010)
12. S. Caravati, M. Bernasconi, M. Parrinello, *J. Phys. Cond. Matt.* **22**, (2010)
13. N. Yamada, *MRS Bulletin* **21** 48 (1996)
14. T. Matsunaga, N. Yamada, *Phys. Rev. B* **69**, 104111 (2004)
15. M. Wuttig, D. Lusebrink, D. Wamwangi, W. Welnic, M. Gillessen, R. Dronskowski, *Nat. Mater.* **6**, 122 (2007)
16. R. Dronskowski, P. E. Blöchl, *J. Phys. Chem.* **97**, 8617 (1993)
17. U. V. Waghmare, N. A. Spaldin, H. C. Kandpal, R. Seshadri, *Phys. Rev. B* **67**, 125111 (2003)
18. R. P. Stoffel, V. L. Deringer, R. E. Simon, R. P. Hermann, R. Dronskowski, *J. Phys. Cond. Matt.* **27**, 085402 (2015)
19. T. Siegrist, P. Jost, H. Volker, M. Woda, P. Merkelbach, C. Schlockermann, M. Wuttig, *Nat. Mater.* **10**, 202 (2011)
20. A. Edwards, A. Pineda, P. Schultz, M. Martin, A. Thompson, H. Hjalmarson, C. Umrigar, *Phys. Rev. B* **73**, 045210 (2006)
21. S. Caravati, M. Bernasconi, T. D. Kühne, M. Krack, M. Parrinello, *J. Phys. Cond. Matt.* **21** 255501 (2009)
22. H. Volker, P. Jost, M. Wuttig, *Adv. Funct. Mater.* , DOI: 10.1002/adfm.201500830 (2015)
23. W. Zhang, A. Thiess, P. Zalden, R. Zeller, P. H. Dederichs, J. Y. Raty, M. Wuttig, S. Blügel, R. Mazzarello, *Nat. Mater.* **11**, 952 (2012)
24. S. Caravati, M. Bernasconi, T. D. Kühne, M. Krack, M. Parrinello, *Appl. Phys. Lett.* **91**, 171906 (2007)
25. J. Akola, R. Jones, *Phys. Rev. B* **76**, 235201 (2007)
26. J. Hegedüs, S. R. Elliott, *Nat. Mater.* **7**, 399 (2008)
27. J. Akola, R. Jones, *Phys. Rev. B* **79**, 134118 (2009)
28. M. Xu, Y. Q. Cheng, L. Wang, H. W. Sheng, Y. Meng, W. G. Yang, X. D. Han, E. Ma, *PNAS* **109**, E1055 (2012)
29. A. V. Kolobov, P. Fons, A. I. Frenkel, A. L. Ankudinov, J. Tominaga, T. Uruga, *Nat. Mater.* **3**, 703 (2004)
30. M. Xu, Y. Cheng, H. Sheng, E. Ma, *Phys. Rev. Lett.* **103**, 195502 (2009)
31. R. Mazzarello, S. Caravati, S. Angioletti-Uberti, M. Bernasconi, M. Parrinello, *Phys. Rev. Lett.* **104**, 085503 (2010)
32. M. Micoulaut, J. Y. Raty, C. Otjacques, C. Bichara, *Phys. Rev. B* **81**, 174206 (2010)
33. E. Cho, J. Im, C. Park, W. J. Son, D. H. Kim, H. Horii, J. Ihm, S. Han, *J. Phys. Cond. Matt.* **22**, 205504 (2010)
34. B. Cai, D. A. Drabold, S. R. Elliott, *Appl. Phys. Lett.* **97**, 191908 (2010)
35. A. V. Kolobov, M. Krbal, P. Fons, J. Tominaga, T. Uruga, *Nat. Chem.* **3**, 311 (2011)

36. X.-B. Li, X. Q. Liu, X. Liu, D. Han, Z. Zhang, X. D. Han, H.-B. Sun, S. B. Zhang, *Phys. Rev. Lett.* **107**, 015501 (2011)
37. M. Micoulaut, A. Kachmar, T. Charpentier, *Phys. Stat. Sol. b* **249**, 1890 (2012)
38. M. Krbal, A. V. Kolobov, P. Fons, K. V. Mitrofanov, Y. Tamenori, J. Hegedüs, S. R. Elliott, J. Tominaga, *Appl. Phys. Lett.* **102**, 111904 (2013)
39. K. V. Mitrofanov, A. V. Kolobov, P. Fons, X. Wang, J. Tominaga, Y. Tamenori, T. Uruga, N. Ciocchini, D. Ielmini, *J. Appl. Phys.* **115**, 173501 (2014)
40. V. Deringer, W. Zhang, M. Lumeij, S. Maintz, M. Wuttig, R. Mazzarello, R. Dronskowski, *Angew. Chem. Int. Ed.* **53**, 10817 (2014)
41. V. L. Deringer, A. L. Tchougreeff, R. Dronskowski, *J. Phys. Chem. A* **115**, 5461 (2011)
42. S. Maintz, V. L. Deringer, A. L. Tchougréeff, R. Dronskowski, *J. Comput. Chem.* **34**, 2557 (2013)
43. J. Raty, W. Zhang, J. Luckas, C. Chen, C. Bichara, R. Mazzarello, M. Wuttig, *Nat. Commun.* **6**, 7467 (2015)
44. H.-S. P. Wong, S. Raoux, S. B. Kim, J. Liang, J. P. Reifenberg, B. Rajendran, M. Asheghi, K. E. Goodson, *Proc. IEEE* **98**, 2201 (2010)
45. D. Ielmini, A. L. Lacaita, D. Mantegazza, *IEEE Trans. Electron Devices* **54**, 308 (2007)
46. P. Fantini, S. Brazzelli, E. Cazzini, A. Mani, *Appl. Phys. Lett.* **100**, 013505 (2012)
47. D. Krebs, T. Bachmann, P. Jonnalagadda, L. Dellmann, S. Raoux, *N. J. Phys.* **16**, 043015 (2014)
48. J. Kalikka, J. Akola, R. O. Jones, *Phys. Rev. B* **90**, 184109 (2014)
49. W. Zhang, I. Ronneberger, P. Zalden, M. Xu, M. Salinga, M. Wuttig, R. Mazzarello, *Sci. Rep.* **4**, 6529 (2014)
50. E. R. Meinders, A. V. Mijiritskii, L. van Pieterson, M. Wuttig,
51. T. H. Lee, S. R. Elliott, *Phys. Rev. Lett.* **107**, 145702 (2011)
52. J. Kalikka, J. Akola, J. Larrucea, R. O. Jones, *Phys. Rev. B* **86**, 144113 (2012)
53. I. Ronneberger, W. Zhang, H. Eshet, R. Mazzarello, *Adv. Funct. Mater.*, DOI: 10.1002/adfm.201500849 (2015)
54. A. Laio, M. Parrinello, *PNAS* **99**, 12562 (2002)
55. A. Sebastian, M. Le Gallo, D. Krebs, *Nat. Commun.* **5**, 4314 (2014)
56. J. Orava, A. L. Greer, B. Gholipour, D. W. Hewak, C. E. Smith, *Nat. Mater.* **11**, 279 (2012)
57. R. Jeyasingh, S. W. Fong, J. Lee, Z. Li, K. W. Chang, D. Mantegazza, M. Asheghi, K. E. Goodson, H. S. Wong, *Nano Lett.* **14**, 3419 (2014)
58. Z. Sun, J. Zhou, R. Ahuja, *Phys. Rev. Lett.* **96**, 055507 (2006)
59. J. Da Silva, A. Walsh, H. Lee, *Phys. Rev. B* **78**, 224111 (2008)
60. C. Pauly, M. Liebmann, A. Giussani, J. Kellner, S. Just, J. Sánchez-Barriga, E. Rienks, O. Rader, R. Calarco, G. Bihlmayer, M. Morgenstern, *Appl. Phys. Lett.* **103**, 243109 (2013)

61. D. Loke, T. H. Lee, W. J. Wang, L. P. Shi, R. Zhao, Y. C. Yeo, T. C. Chong, S. R. Elliott, *Science* **336**, 1566 (2012)
62. G. C. Sosso, G. Miceli, S. Caravati, J. Behler, M. Bernasconi, *Phys. Rev. B* **85**, 174103 (2012)
63. G. Sosso, G. Miceli, S. Caravati, F. Giberti, J. Behler, M. Bernasconi, *J. Phys. Chem. Lett.* **4**, 4241 (2013)
64. G. Sosso, J. Colombo, J. Behler, E. Del Gado, M. Bernasconi, *J. Phys. Chem. B* **118**, 13621 (2014)
65. T. Matsunaga, J. Akola, S. Kohara, T. Honma, K. Kobayashi, E. Ikenaga, R. O. Jones, N. Yamada, M. Takata, R. Kojima, *Nat. Mater.* **10**, 129 (2011)
66. M. Salinga, E. Carria, A. Kaldenbach, M. Bornhofft, J. Benke, J. Mayer, M. Wuttig, *Nat. Commun.* **4**, 2371 (2013)
67. P. G. Debenedetti, F. H. Stillinger, *Nature* **410**, 259 (2001)
68. H. Zhang, C.-X. Liu, X.-L. Qi, X. Dai, Z. Fang, S.-C. Zhang, *Nat. Phys.* **5**, 438 (2009)
69. M. Z. Hasan, C. L. Kane, *Rev. Mod. Phys.* **82**, 3045 (2010)
70. J. Kim, J. Kim, S.-H. Jhi, *Phys. Rev. B* **82**, 201312(R) (2010)
71. R. E. Simpson, P. Fons, A. V. Kolobov, T. Fukaya, M. Krbal, T. Yagi, J. Tominaga, *Nat. Nanotechnol.* **6**, 501 (2011)
72. J. Tominaga, A. V. Kolobov, P. Fons, T. Nakano, S. Murakami, *Adv. Mater. Inter.* **1**, 1300027 (2014)
73. B. Sa, J. Zhou, Z. Sun, J. Tominaga, R. Ahuja, *Phys. Rev. Lett.* **109**, 096802 (2012)
74. B. Prasai, M. E. Kordesch, D. A. Drabold, G. Chen, *Phys. Stat. Sol. b* **250**, 1785 (2013)
75. J. M. Skelton, A. R. Pallipurath, T.-H. Lee, S. R. Elliott, *Adv. Funct. Mater.* **24**, 7291 (2014)
76. M. Zhu, M. Xia, F. Rao, X. Li, L. Wu, X. Ji, S. Lv, Z. Song, S. Feng, H. Sun, S. Zhang, *Nat. Commun.* **5**, 4086 (2014)
77. W.-D. Song, L.-P. Shi, X.-S. Miao, C.-T. Chong, *Adv. Mater.* **20**, 2394 (2008)
78. D. Ding, K. Bai, W. D. Song, L. P. Shi, R. Zhao, R. Ji, M. Sullivan, P. Wu, *Phys. Rev. B* **84**, 214416 (2011)
79. W. Zhang, I. Ronneberger, Y. Li, R. Mazzarello, *Adv. Mater.* **24**, 4387 (2012)
80. J. M. Skelton, S. R. Elliott, *J. Phys. Cond. Matt.* **25**, 205801 (2013)
81. A. L. Greer, *Nat. Mater.* **14**, 542 (2015)
82. K. S. Novoselov, V. I. Fal'ko, L. Colombo, P. R. Gellert, M. G. Schwab, K. Kim, *Nature* **490**, 192 (2012)
83. Q. H. Wang, K. Kalantar-Zadeh, A. Kis, J. N. Coleman, M. S. Strano, *Nat. Nanotechnol.* **7**, 699 (2012)
84. T. Hickel, A. Dick, B. Grabowski, F. Körmann, J. Neugebauer, *Steel Res. Int.* **80**, 4 (2010)
85. K. Nomura, H. Ohta, A. Takagi, T. Kamiya, M. Hirano, H. Hosono, *Nature* **432**, 488 (2004)